2002

Studies on Capacity Fade of Spinel-Based Li-Ion Batteries

Ramadass Premanand
University of South Carolina - Columbia

Anand Durairajan
University of South Carolina - Columbia

Bala Haran
University of South Carolina - Columbia

Ralph E. White
University of South Carolina - Columbia, white@cec.sc.edu

Branko N. Popov
University of South Carolina - Columbia, popov@engr.sc.edu

Publication Info

Journal of the Electrochemical Society, 2002, pages A54-A60.

Publisher's link: http://dx.doi.org/10.1149/1.1426399
DOI: 10.1149/1.1426399

Journal of The Electrochemical Society, **149** (1) A54-A60 (2002)
0013-4651/2001/149(1)/A54/7/$7.00 © The Electrochemical Society, Inc.

Studies on Capacity Fade of Spinel-Based Li-Ion Batteries

Ramadass Premanand, Anand Durairajan,* Bala Haran, Ralph White,*** and Branko Popov**,z**

Department of Chemical Engineering, University of South Carolina, Columbia, South Carolina 29208, USA

The performance of Cell-Batt® Li-ion cells using nonstoichiometric spinel as the positive electrode material has been studied at different charging rates. The capacity of the cell was optimized based on varying the charging current and the end potential. Subsequent to this, the capacity fade of these batteries was studied at different charge currents. During cycling, cells were opened at intermittent cycles and extensive material and electrochemical characterization was done on the active material at both electrodes. For all charge currents, the resistance of both the electrodes does not vary significantly with cycling. This result is in contrast with cells made with $LiCoO_2$ cathode where the increase in cathode resistance with cycling causes the fade in capacity. Comparison of cyclic voltammograms of spinel and carbon electrode before and after 800 cycles reveals a decrease in capacity with cycling. Low rate charge-discharge studies confirmed this loss in capacity. The capacity loss was approximately equally distributed between both electrodes. On analyzing the X-ray diffraction patterns of the spinel electrode that were charged and discharged for several cycles, it can be seen that apart from the nonstoichiometric spinel phase, an additional phase slowly starts accumulating with cycling. This is attributed to the formation of defect spinel product λ-MnO_2 according to a chemical reaction, which also leads to MnO dissolution in the electrolyte. Energy dispersive analysis by X-ray of the carbon samples shows an increase in Mn content with cycling. These studies indicate that capacity fade of spinel-based Li-ion cells can be attributed to (*i*) structural degradation at the cathode and (*ii*) loss of active materials at both electrodes due to electrolyte oxidation.
 [DOI: 10.1149/1.1426399]

Manuscript submitted May 31, 2001; revised manuscript received August 15, 2001. Available electronically December 10, 2001.

It is well known that the capacity of a lithium-ion battery decreases during cycling and most of the loss can be associated with some unwanted side reactions that occur in these batteries during overcharge and over discharge conditions.[1] These reactions may cause electrolyte decomposition, passive film formation, active material dissolution, phase changes in the insertion electrode, and several other phenomena.

Carbonaceous anode materials in lithium-ion rechargeable cells exhibit irreversible capacity loss in the first cycle, mainly due to reaction of lithium during the formation of passive surface films.[2] Passivation of the carbon electrode during the formation period and subsequent capacity loss are highly dependent on specific properties of carbon in use, such as degree of crystallinity, surface area, and so on. Positive electrode dissolution phenomena are both electrode and electrolyte specific and the factors that determine the positive electrode dissolution are structural defects in the positive active material, high charging potentials, and several other phenomena.[1] Oxygen defects in the electrode material may weaken the bonding force between the transition metal and oxygen resulting in the metal dissolution.

Previously, capacity fade studies were done on commercially available lithium-ion cells with $LiCoO_2$ as the positive material.[3] These studies revealed that the positive electrode contributes more to the capacity fade of the lithium ion cells, when compared to the negative electrode and the increase in impedance of $LiCoO_2$ electrode with cycling is the dominant factor for loss in capacity of the battery. In this paper an attempt was made to study the capacity fade of commercially available spinel-based lithium-ion batteries and also to optimize the charging current based on charging time and capacity fade.

Commercially produced Li-ion cells include several features for safe operation under different conditions. During charging, to prevent electrolyte oxidation a potential limit (charging to ultimate voltage) is used with internal electrical circuitry (cell voltage control and equalization circuit).[4] However, different charging protocols lead to different charging times. Further, varying the charge protocol also affects the capacity fade during cycling.[1] One of the commonly used charging protocol for Li-ion cells is charging at constant current to a particular voltage and subsequently holding the potential constant. In this case, the total time for charging is held constant. One of the drawbacks of this process is that, since the total charging time is constant, the battery is held at a high constant voltage for longer than essential. In this case, holding the cell potential at high voltage can contribute to oxidation of the cathode leading to capacity decay during cycling.

Optimization of charging protocol is essential to achieve superior performance for the Li-ion batteries. Objectives of this paper were to study the performance of lithium-ion batteries with spinel-based cathodes. First, we want to optimize the discharge capacity of the cell based on the charge current, end potential, and total charging time. Next, we compare the capacity fade of cells charged at different rates to a common end potential and discharged at the same current. The goal here is to minimize the capacity loss with cycling by choosing an optimum charging current. Finally, we study the causes for the capacity fade in spinel based Li-ion batteries.

Experimental

All studies were done on Cell-Batt Li-ion cell (obtained from International Battery Technologies) with an initial capacity of 1050 mAh at room temperature. Table I presents the cell characteristics. The charging protocol involved applying the constant current (CC) and constant voltage (CV) method. As mentioned in the introduction, one of the common methods of charging Li-ion cells involves applying a constant current to a predetermined cutoff potential, following which the potential is held constant till the total charging time is 3 h.

For example, using this protocol cells are charged at 1 A from 3 to 4.2 V and subsequently the potential is held constant at 4.2 V till the total charging time is 3 h. The drawbacks of this approach are: (*i*) inefficiency during charge since lithiation/delithiation processes at the anode and cathode could have ended much earlier than 3 h and (*ii*) loss of active material due to oxidation of both electrolyte and the positive electrode at the high potential. In this paper, we used a modified form of the CC-CV protocol. Instead of holding the charging time constant, we monitor the decay in current with time during the constant voltage part. When the current reaches 50 mA, we stop charging. In order to establish the optimum cutoff voltage, cells were charged at a constant current of 1 A to different end voltages. The potential was held constant till the current decayed to 50 mA. Subsequently the cells were discharged at a constant current of 1 A.

* Electrochemical Society Student Member.
** Electrochemical Society Active Member.
*** Electrochemical Society Fellow.
z E-mail: popov@engr.sc.edu

Table I. Physical characteristics of Cell-Batt lithium-ion battery electrodes.

Characteristics	Positive spinel	Negative carbon
Mass of the electrode material, g	9.592	5.0865
Geometric area (both sides), cm^2	436	498
Loading on one side, mg/cm^2	22	10.2
Thickness of the electrode, μm	91	70
Dimensions of the electrode, cm × cm	54.5 × 4	58.5 × 4

Figure 1 shows the discharge profiles for Cell-Batt cells charged to various cutoff potentials. It is seen from the plot that the discharge capacity increases with cutoff potential. A maximum is seen at 4.17 V beyond which no further increase in capacity is seen. The time expended during the constant current and constant voltage part while charging to different cutoff voltages is presented in Table II. The open-circuit voltage of the cell in the discharged state is around 3.0 V. For 1 A charge, the cell voltage reaches 4 V within 325 s, and the battery is charged for the most part at constant voltage. Similar results are also seen for 4.05 and 4.10 V. However, as seen from Fig. 1 these voltages are insufficient for completely charging the battery. Increasing the cutoff voltage to 4.17 V results in completely charging the cell as seen by the significant increase in discharge capacity. Increasing the cutoff voltage further to 4.3 V decreases the constant voltage time. Similarly, the total charging time decreases as compared to that for the cell charged to 4.17 V.

Since, no difference in capacity is seen between charging at 4.17 V and 4.3 V, in subsequent studies the cell was charged to 4.17 V. This was done primarily to prevent oxidation of the electrolyte and the spinel. According to Aurbach *et al.*,[5] cycling spinel in the potential range 3.5-4.2 V caused no Mn dissolution. Based on this observation the protocol consisted of the following steps: (*i*) initially, the battery was charged at a constant current till the potential reached 4.17 V, (*ii*) next, the cell voltage was held constant at 4.17 V and the current was monitored. Charging was stopped when the current reached 50 mA. Batteries after different charge-discharge cycles were analyzed using impedance spectroscopy and linear polarization. Some batteries were cut open and both positive and negative electrodes were analyzed using X-ray diffraction (XRD), scanning electron microscopy (SEM), and energy dispersive analysis by X-ray (EDAX). Solartron SI 1255 HF frequency response analyzer and potentiostat/galvanostat model 273A were used for the electrochemical characterization studies. Charge-discharge studies were

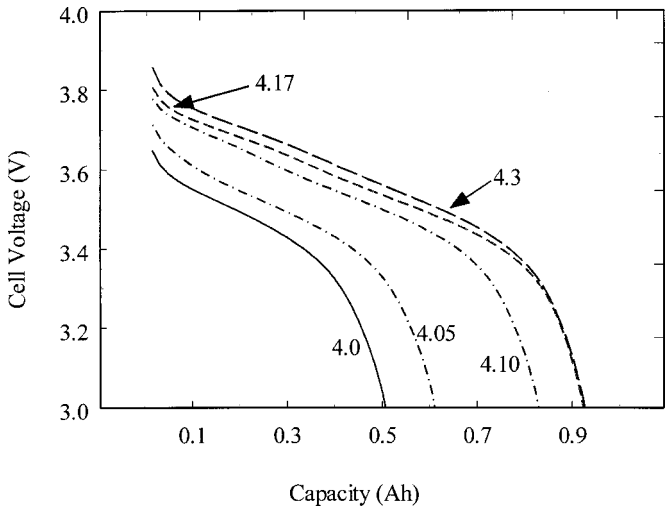

Figure 1. Change in discharge capacity for Li-ion cells charged to different potentials.

Table II. Comparison of charging time for Li-ion cells charged to different cutoff voltages.

	Charging time (h)		
Cutoff voltage (V)	CC[a] time	CV[b] time	Total time
4.00	0.09	1.74	1.83
4.05	0.13	2.08	2.21
4.10	0.17	3.04	3.21
4.17	0.24	2.08	2.32
4.30	0.49	0.92	1.41

[a] Constant current.
[b] Constant voltage.

carried out in the potential range of 3.0-4.2 V. The cells were left on open circuit for 1 h and after the potential stabilized, impedance studies were performed. The cell was stable during the experiments, and its voltage changed less than 1 mV. Electrical impedence spectroscopy (EIS) measurements were done on the cells at both charged and discharged states. The impedance data generally covered a frequency range of 0.001 to 10,000 Hz. A sinusoidal ac voltage signal varying by ±5 mV was applied.

The following studies were done to understand the process occurring at individual electrodes of the cell. The can of fresh and cycled cells was carefully opened at fully discharged state in a glove box filled with ultrapure argon (National Gas and Welders, Inc.). The term ''fresh electrode'' refers to the electrode of the Cell-Batt battery when it is bought. It is well known that commercial cells are already preconditioned before reaching the public. Hence, the irreversible capacity loss in the negative electrode was taken care while preconditioning itself. Next, pellet electrodes were made from the positive and negative electrodes and were used as working electrodes in the T-cell. Pure lithium metal was used as the counter and reference electrode. A separator taken from the battery was used as a separator in the T-cell. The diameter of the pellet electrodes was 1.20 cm, and the ratio of area of the disk electrode to original electrode area was 0.00243. 1 M $LiPF_6$ was used as the electrolyte in a 1:1 mixture of ethylene carbonate (EC) and dimethyl carbonate (DMC). EIS studies were done on the T-cells to understand the influence of positive and negative electrodes on the total impedance of the cell. Impedance was measured at both charged and discharged states. The frequencies of the ac signal ranged from 10 kHz to 0.005 Hz.

Results and Discussion

Figure 2 presents the change in current (Fig. 2a) and potential (Fig. 2b) during charging the Cell-Batt cell at four different currents. At the negative electrode of a Li-ion cell $Cu|Li_xC|Li^+|Li_\alpha(Mn_{2-\gamma}Li_\gamma)O_4|Al$, the following electrochemical reaction occurs

$$Li_xC + \delta Li^+ + \delta e^- \underset{\text{Discharge}}{\overset{\text{Charge}}{\rightleftarrows}} Li_{x+\delta}C \qquad [1]$$

while at the positive electrode the reaction is

$$Li_\alpha(Mn_{2-\gamma}Li_\gamma)O_4 \underset{\text{Discharge}}{\overset{\text{Charge}}{\rightleftarrows}} Li_{\alpha-\delta}(Mn_{2-\gamma}Li_\gamma)O_4 + \delta Li^+ + \delta e^- \qquad [2]$$

During charge Li^+ intercalates into the carbon electrode (reduction), and the anode potential moves closer to 0 from 1.2 V. Simultaneously, the spinel is oxidized (deintercalation) and its potential changes from 3.0 to 4.2 V. During discharge, the reverse of the above happens. Comparing the different charge rates (0.25, 0.5, 0.75, and 1 A) we can see that increasing the charge current keeps the battery in the constant potential mode during most of the charge. The decay in current with time is similar for different charging rates.

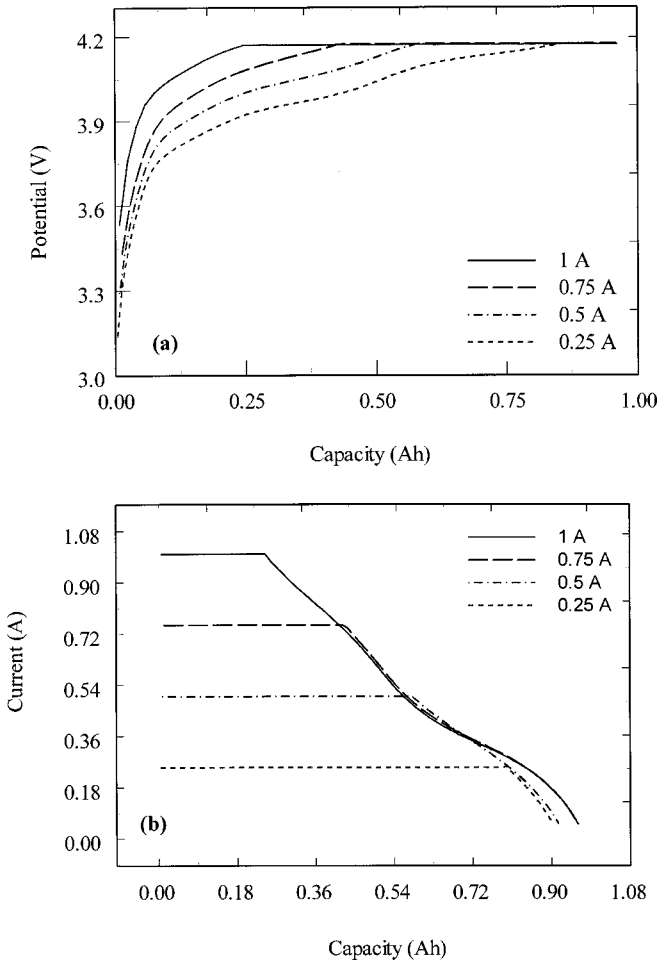

Figure 2. Change in current (a, top) and potential (b, bottom) with capacity at different charge rates.

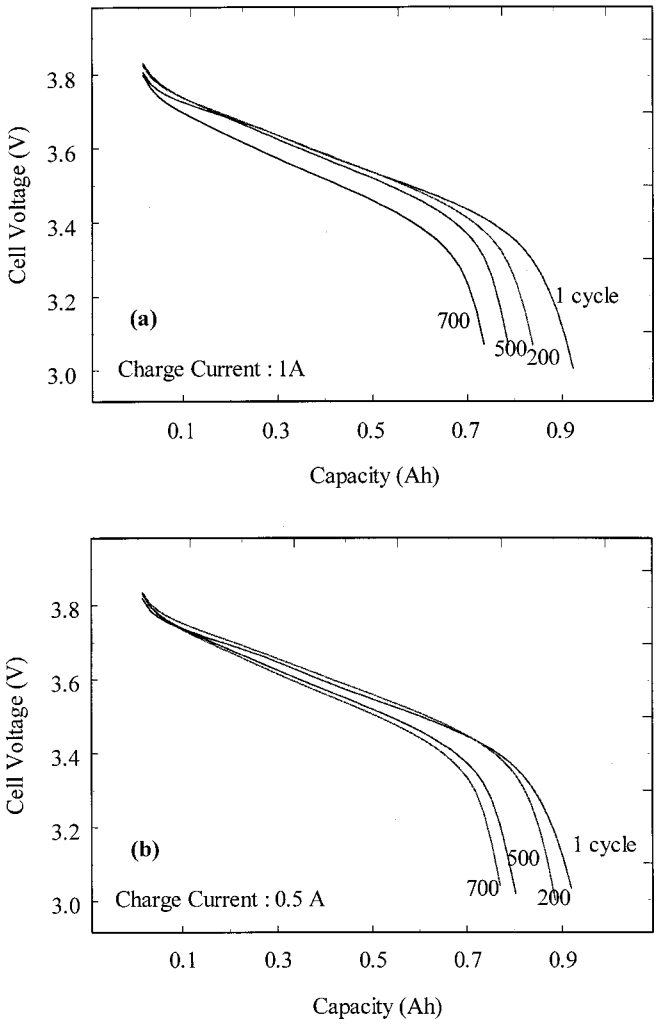

Figure 3. Discharge curves of batteries cycled at 1 A (a, top) and 0.5 A (b, bottom) at different cycles.

The cell potential of the Li-ion cell can be represented as

$$V = E_0 - \mathrm{I}(R_\Omega + R_\mathrm{P}) \quad [3]$$

where E_0 is the concentration-dependent equilibrium potential, I is the charge current, R_Ω is the electrolyte resistance, and R_p is time-dependent and is the sum of cathode and anode resistances.

Table III presents the CC and CV charging time for cells cycled at different currents after 100 cycles. The discharge capacity of the cells does not vary significantly. In Eq. 3, increasing the charge current results in increasing the value of R_p due to the increase in the cathode and anode mass-transfer resistances. Hence, the cell reaches 4.17 V faster at higher charge currents. This is experimentally seen in Table III, where the CC time decreases and CV time increases with increase in charge current. From Eq. 3, it is clear that increasing the charge current (I) leads to the battery reaching the constant potential plateau of 4.17 V faster. Hence, increasing the charging current keeps the battery in the constant voltage mode during most part of the charge. It is evident that the total charging time (CC + CV time) is more for cells cycled at lower currents. However, increasing the charging rate above 0.5 A does not decrease the total time significantly.

Table III. Comparison of charging time for Li-ion cells charged at different currents.

Charge current (A)	Charging time (h)		Total time (h)
	CC time	CV time	
0.10	8.66	0.27	8.94
0.25	3.04	0.87	3.90
0.50	1.14	1.44	2.58
0.75	0.55	1.85	2.40
1.00	0.19	2.03	2.22

From Table III, it is clear that varying the charging current from 0.5 to 1 A, does not lead to any significant savings in the total charging time. However, for all three currents, the CC and CV times vary significantly. This can lead to differing capacities with cycling. The goal is to minimize capacity fade without increasing charging time. Hence, our next objective was to compare the capacity fade behavior of cells charged at different currents.

All batteries were discharged at a constant current of 1 A to a cutoff potential of 3.0 V. Since the discharge rates for all batteries remained the same, any variation in capacity decay with cycling should be due to the change in charging current.

Figure 3 presents the discharge curves at different cycles for charging at 1 A (Fig. 3a) and 0.5 A (Fig. 3b). From the plot it is clear that increasing the charging rate, increases the capacity fade of the batteries. For the battery charged at 0.5 A, a capacity fade of 15.4% is seen after 800 cycles. For the battery charged at 1 A, a capacity fade of 18.29% is seen after 800 cycles.

Figure 4 presents a comparison of the charge curves for cells charged at 0.5 and 1 A after 200 and 500 cycles. At both cycles, the capacity fade is lesser for the cell cycled at 0.5 A. Since, the total

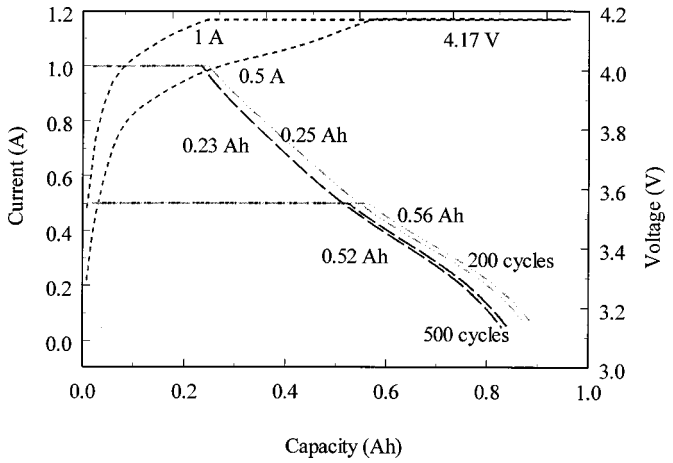

Figure 4. Comparison of charge curves for cells charged at 1 A and 0.5 A after 200 and 500 cycles.

charging time is comparable for cells charged at 0.5 and 1 A, Fig. 4 shows that the capacity fade can be minimized by optimizing the charging current. In Fig. 4, the constant voltage part is reached at capacities of 0.56 and 0.25 Ah at charge currents of 0.5 and 1 A, respectively, after 200 cycles. The battery was charged in the constant voltage mode 74% of the time at 1 A rate and 41% of the time at 0.5 A rate.

Figure 5 presents the capacity fade for cells charged at different rates. It is seen that the capacity decay is at a minimum for charging at 0.5 A. Increasing the charging rate further results in additional decrease in capacity. From Fig. 5 and Table III, it is clear that 0.5 A gives the best performance in terms of minimum capacity loss and optimum charging time for these cells. Comparing the total charging time for different charging currents, it is seen that the total time decreases with cycling. This is to be expected since the capacity of the cell decays continuously. After 500 cycles, the difference in total charging time for cells charged at 1 and 0.5 A is around 350 s. However, the loss in capacity is higher for the cell charged at 1 A, 12.5% and 13.5% decay for 0.5 A and 1 A charge, respectively. Figure 6 presents the fraction of time the cell is charged in the constant current mode as a function of cycle life. The total charging time as a function of cycle life is given in Table IV. For all charge rates, both the constant current and constant voltage charging time decrease with cycling. However as seen in Fig. 6, the percentage of the total time, which goes for constant current charging, remains approximately the same with cycle life.

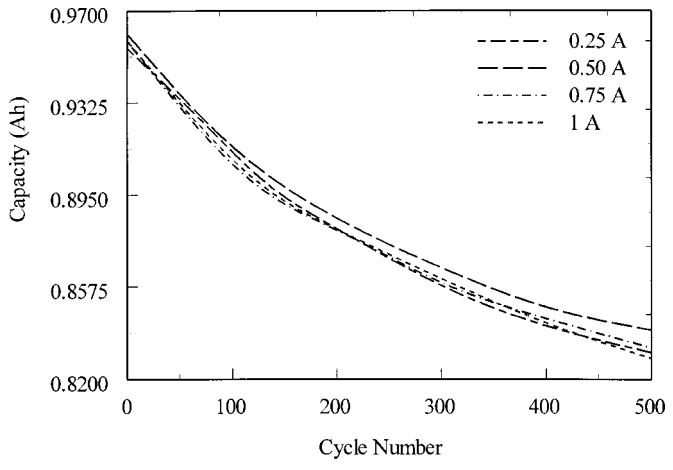

Figure 5. Capacity fade of Li-ion cells charged at different currents.

Table IV. Change in total charging time with cycling.

	Total charging time (h)			
Cycle no.	0.25 A	0.5 A	0.75 A	1 A
1	3.92	2.72	2.46	2.32
100	3.91	2.69	2.46	2.26
200	3.91	2.67	2.32	2.14
300	3.9	2.64	2.32	2.11
400	3.9	2.61	2.3	2.07
500	3.83	2.46	2.28	2.07

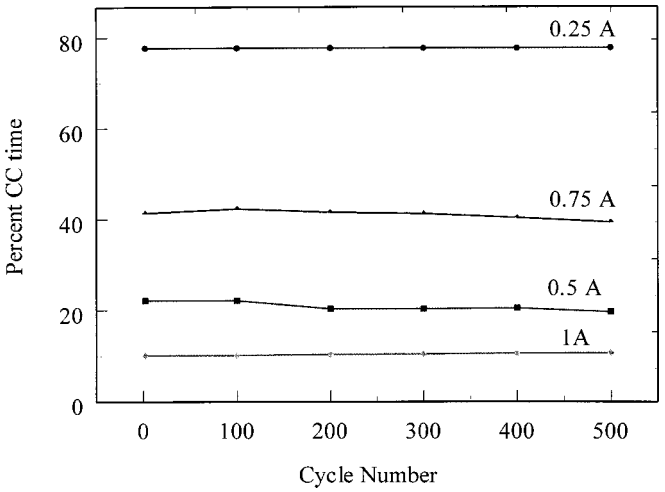

Figure 6. Variation in constant current charging time as a function of cycle life.

In order to understand the effect of charging rate on capacity fade, it is important to review the behavior of spinel and carbon in $LiPF_6$-EC-DMC. Capacity decay of spinel has been studied extensively in literature. Gummow *et al.*[6] first ascribed the capacity fading of spinel to the dissolution of Mn into the electrolyte solution. Huang *et al.*[7] have correlated the capacity loss of stoichiometric and nonstoichiometric spinel to electrode structural integrity. The rapid decay in capacity of stoichiometric spinel is caused due to the formation of λ-MnO_2, which forms upon extraction of lithium, accumulates during cycling, and becomes disconnected from the electrode. However, in our case the electrode is nonstoichiometric in nature, as it does not exhibit such rapid fade in capacity on cycling. Xia *et al.*[8] attribute capacity fade of spinel-based Li-ion battery to transformation of unstable two-phase spinel to a more stable one-phase structure via loss of MnO. They find that this effect becomes more pronounced at high temperatures. While the capacity loss of the whole battery is generally ascribed to the spinel cathode, recent investigations reveal that the storage loss at high temperatures arises due to the carbon anode. According to Wang *et al.*[9] at high temperatures, capacity loss of a charged lithium ion cell is due to loss of cyclable lithium ions at the carbonaceous anode, as a result of acid generated at the cathode. In light of the recent evidence, the capacity loss can be due to either the spinel or the carbon anode.

In order to analyze the cause for the capacity fade of spinel-based Li-ion cells impedance analysis was done. Figure 7 presents the change in cell resistance as a function of state of charge (SOC). It is evident that the cell impedance decreases with the increase in SOC. During charge, lithium deintercalates from the spinel electrode, thereby increasing its conductivity. Similarly, lithium intercalation into carbon increases its conductivity. Hence, the cell impedance varies with SOC. Rearranging Eq. 3 and multiplying by time gives

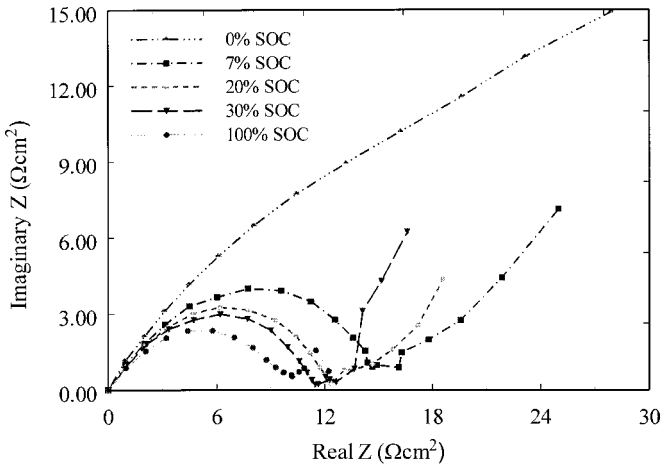

Figure 7. Nyquist plots for a Cell-Batt cell charged at 0.5 A at different states of charge.

$$Idt = \frac{(E_0 - V)dt}{R_\Omega + R_P} \quad [4]$$

At cutoff conditions, the terminal voltage of the battery is the cutoff voltage, and It_{cut} is the discharge capacity (Q) of the battery. That is

$$Q = It_{cut} = \int_0^{t_{cut}} \frac{(E_0 - V)}{R_\Omega + R_P} dt \quad [5]$$

During the galvanostatic discharge process, E_0 decreases and R_p increases (see Fig. 7). The cell ohmic resistance R_Ω does not vary with SOC. Due to an increase in R_p and decrease in E_0, the cell voltage drops to its cutoff voltage V_{cut}. Changes in the anode and cathode resistance and the cell emf are directly dependent on the lithium content. In a previous paper,[3] we had presented results on impedance analysis of carbon and $LiCoO_2$ electrodes at different charge-discharge cycles. It was seen that the primary cause for capacity fade was the increase in resistance at the cathode ($LiCoO_2$).[3] From Eq. 5 it is clear that increased electrode resistance can contribute to lower capacity. Figure 8 presents the cell impedance of the 0.5 A charged battery at different cycles. Impedance results show that the cell impedance increases with cycling. Figure 9a and b present the impedance of individual electrodes in the discharged state. The overall resistance of the carbon electrode is slightly larger

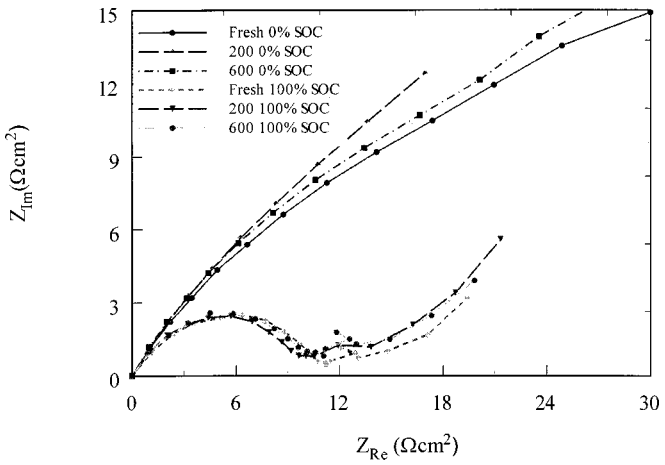

Figure 8. Variation in total cell impedance of Cell-Batt battery at different charge-discharge cycles. The cell was charged at 0.5 A.

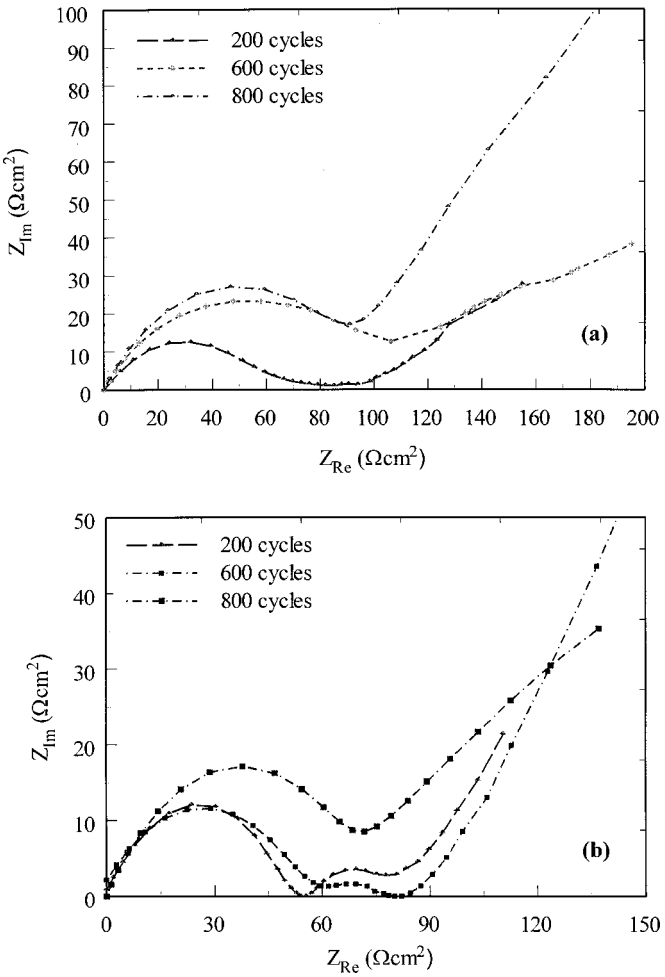

Figure 9. Nyquist plots obtained using a T-cell at discharged state for carbon (a, top) and spinel (b, bottom).

than that of the spinel. With continuous cycling there is no significant change in the overall impedance for both the electrodes. Similar results are observed for cells charged at different currents. Since, no significant increase in resistance is observed, this does not account for the large capacity decay (15-19% for 500 cycles) seen with cycling. This is also confirmed by rate capability studies done on a battery cycled 1000 times. If an increase in cell resistance were significant, it would coincide with a similar loss of rate capability. This is in contrast to $LiCoO_2$-based cells where resistance at the cathode controls overall battery performance[10] and is responsible for the capacity fade with cycling.[3]

Capacity fade can also arise due to the loss of electrical contact among some of the particles from the bulk of the electrode. Comparison of discharge curves and impedance of individual electrodes with that of the battery proves that loss of contact among the particles does not cause the capacity fade. Another reason for capacity fade could be the loss of active material because of formation of oxidation products at the particle/electrolyte interface. According to Aurbach *et al.*,[5] the onset of electrolyte oxidation (EC-DMC) in Li-ion cells may be as low as 3.7 V. This oxidation process of the solution produces a sufficient concentration of Lewis acids, which interact with the active mass and lead to its partial dissolution. The generation of Lewis acids has been observed irrespective of the type of cathode used.[9] Acid generation leads to Mn disproportionation and dissolution in the electrolyte during normal cycling. Since electrolyte oxidation starts at 3.7 V, the amount of oxidation products generated depends on the charge current and the charging time. At low rates, although the charge current is small the total charging

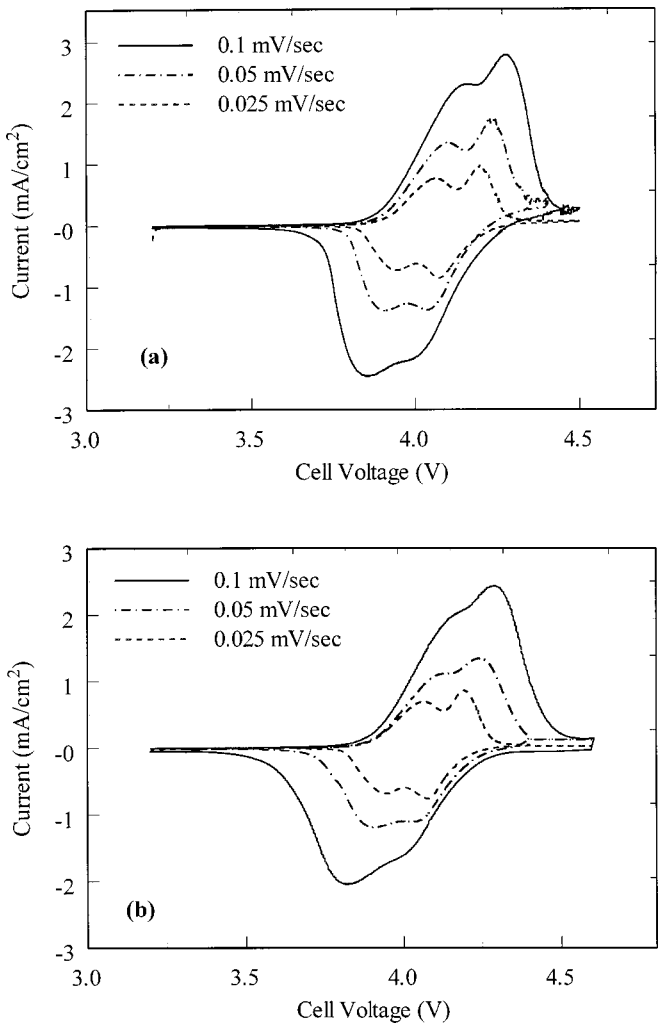

Figure 10. Cyclic voltammograms of spinel electrodes: fresh (a, top) and after 800 cycles (b, bottom) at different scan rates.

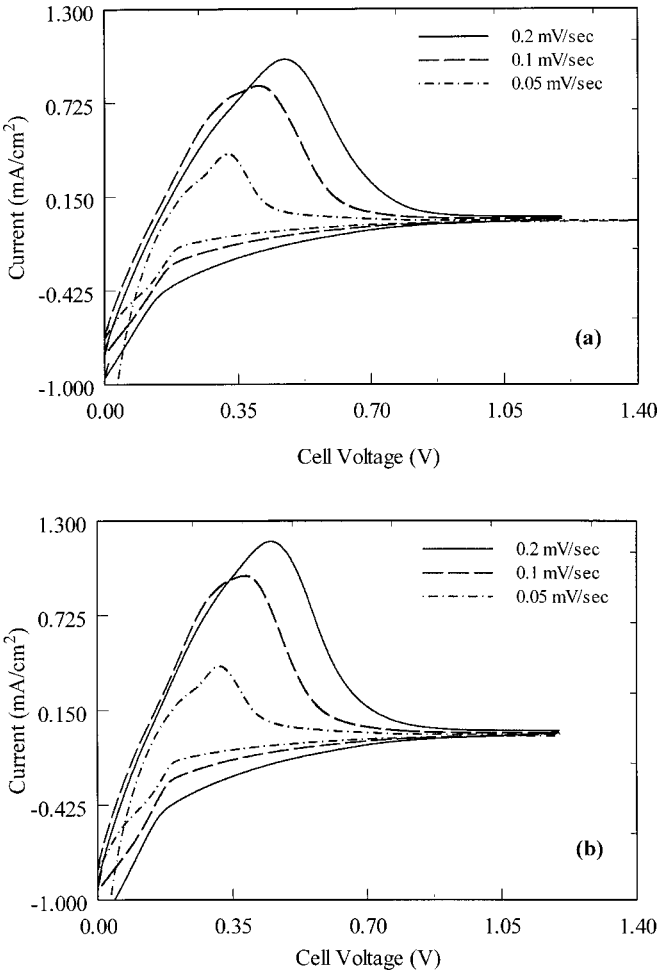

Figure 11. Cyclic voltammograms of carbon electrodes: fresh (a, top) and after 800 cycles (b, bottom) at different scan rates.

time is long. From Table III, at a current of 0.25 A, the cell is charged for a total time of roughly 9 h. Since the total charging time is long, the capacity fade is larger than that observed at 0.5 A.

As the electrode is kept for longer periods of time at 4.17 V at higher charge rates (>0.5 A), this could cause more oxidation of the electrolyte. For the same reason, at a given charge rate increasing the end-of-charge voltage causes more capacity fade. After 100 cycles, the capacity loss at a cutoff potential of 4.17 V is 4.51% while that for 4.3 V is 4.95%. These results indicate that for cycling commercial spinel-based Li-ion cells, it is essential to optimize both the charging current and the end-of-charge voltage.

In order to study changes in the electrode structure due to cycling, cyclic voltammetry was done on individual carbon and spinel electrodes taken from fresh cells and cells cycled 800 times. Figure 10 presents cyclic voltammograms (CVs) of spinel electrodes at different cycles. The two characteristic peaks for spinel are clearly seen at low sweep rates. As seen from the plot, increasing the scan rate results in shifting the peak potential to more positive values during the forward sweep and to more negative values during the reverse sweep. Similar results are seen for spinel after 800 charge-discharge cycles. Comparison of Fig. 10a and b, indicates that the magnitude of the peak currents for Li intercalation and deintercalation have diminished with cycling. The peak currents appear at the same voltages for both the fresh and cycled electrode. This indicates that the thermodynamics of Li intercalation into the electrode has not changed due to cycling. Since, the electrode resistance has not changed significantly with cycling, the reduction in the peak current is attributed to loss of active spinel.

Figure 11 presents cyclic voltammograms obtained for the carbon electrode using a T-cell. The potential was initially swept from 1.2 to 0 V and then back during the reverse sweep. The forward scan (sweep to 0 V) corresponds to Li^+ intercalation into carbon and is equivalent to charging the Li-ion cell. Increasing the sweep rate results in increasing the peak current during both forward and reverse scans. Further, during the forward sweep the peak potential appears at more positive potentials as the scan rate is increased. Similar to Fig. 10, the peak currents decrease in magnitude with cycling. This was also confirmed by low rate charge-discharge studies on both the spinel and carbon electrodes. For the spinel electrode taken from a fresh battery delithiation for 14 h at 10 mA/g gives a capacity of 140 mAh/g. These results were compared with spinel active material from a cell cycled 800 times. In this case, delithiation for 15.3 h at 7.84 mA/g gives a capacity of 120 mAh/g. Similar capacity losses were observed for the carbon electrode also. To study changes in electrode structure with cycling XRD and EDAX analysis were done.

In order to confirm the CV data, XRD was done on the carbon and spinel electrodes at 200, 400, 600, and 800 cycles. The patterns were collected at the end of discharge with a Tigaku 405S5 X-ray diffractometer using Cu Kα radiation. X-ray data was also done on spinel and carbon from a fresh cell. Figure 12 shows the powder XRD patterns of the spinel samples taken out of the Cell-Batt battery charged at 0.5 A at different cycles. After 800 cycles additional phases of Li-Mn compounds are seen in the diffraction patterns.

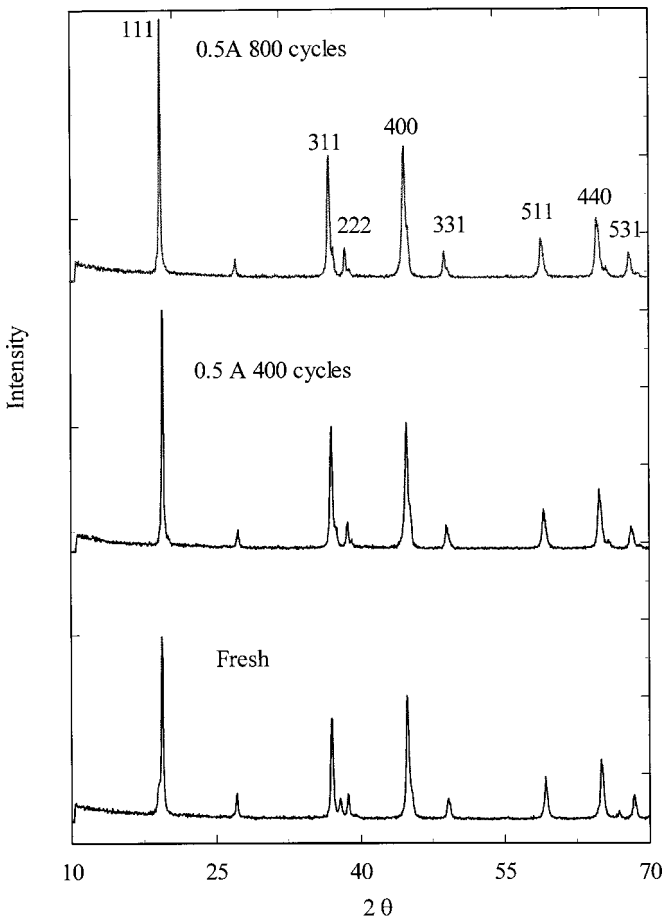

Figure 12. XRD patterns of spinel after different charge-discharge cycles. $LiMn_2O_4$ was taken from Cell-Batt battery charged at 0.5 A.

There are an infinite number of compositions in the $LiMn_2O_4$-$Li_2Mn_4O_9$-MnO_2 tie triangle of the Li-Mn phase diagram; all these materials have lattice parameters between 8.24 and 8.03 Å. Therefore, there will be many different compositions that will yield the same lattice parameter, which is dependent on the Li and Mn content in the various structures. The best match we got from the database was found to be $Li_{0.82}[Mn_{1.7}Li_{0.3}]O_4$. With cycling the spinel peaks shift slightly to the right, which indicates a contraction in the lattice parameter. According to Cho and Thackeray[11] all spinel compounds within the $LiMn_2O_4$-$Li_2Mn_4O_9$-λ-MnO_2 tie line triangle have lattice constants smaller than $LiMn_2O_4$ as the latter has the highest concentration of the relatively large Mn^{3+} ion (ionic radius of Mn^{3+} = 0.65 Å; ionic radius of Mn^{4+} = 0.53 Å). This can be verified by means of a lattice parameter calculation of the unit cubic cell on the basis of the 440 diffraction peak.[7] The shift in peaks to higher 2θ values and the small reduction in the lattice constant from 8.17 to 8.13 Å after 800 cycles indicate compositional changes with cycling. On analyzing the XRD patterns of the electrode that were charged and discharged for several cycles, it can be seen that apart from the nonstoichiometric spinel phase, an additional phase slowly starts accumulating with cycling. This could be due to formation of defect spinel product λ-MnO_2 according to the chemical reaction

$$2LiMn_2O_4 \rightarrow 3\lambda - MnO_2(\text{solid}) + MnO(\text{solution}) + Li_2O(\text{solution}) \quad [6]$$

as proposed by Hunter.[12]

The MnO dissolved in the solution is deposited on the carbon anode. This was confirmed by EDAX analysis for the carbon samples taken after different charge-discharge cycles. Up to 200 cycles the presence of manganese over the surface of carbon is very negligible. However, from the EDAX analysis of the samples taken after 400, 600, and 800 cycles, it can be seen that the Mn content increases with cycling. Although, EDAX is qualitative in nature the presence of Mn on the carbon surface indicates Mn dissolution due to electrolyte oxidation during charge and deposition on the anode during subsequent cycles. The acid generated during electrolyte oxidation also attacks the solid electrolyte interphase (SEI) film formed on the carbon surface. Hence, the capacity fade of the spinel-based Li-ion cells can be attributed to loss of active materials at both electrodes due to electrolyte oxidation.

Conclusions

Capacity fade of commercial Li-ion cells (Cell-Batt) with spinel cathodes has been studied at different charge rates. The charging protocol consisted of constant current charging to 4.17 V and subsequently holding the potential constant at the same value till the current decayed to 50 mA. All cells were discharged at a constant current of 1 A to 3 V. By comparing cells charged at different currents we can see that increasing the charging rate keeps the battery in the constant potential mode during most part of the charge. The decay in current with time during the constant voltage part is similar for different charging rates. To study the cause for the capacity fade of spinel-based Li-ion cells, impedance analysis, cyclic voltammetry, and XRD analysis were done. Impedance studies reveal no significant increase in resistance at both electrodes after 800 charge-discharge cycles. Cyclic voltammograms and charge-discharge studies show that Li intercalation and deintercalation kinetics has diminished with cycling. Since, the electrode resistance does not change with cycling, the reduction in peak currents indicates loss in active material at both electrodes. XRD studies of spinel electrode reveal the formation of an additional phase with cycling. This is attributed to λ-MnO_2 which also leads to dissolution of Mn in the electrolyte. EDAX analysis of the carbon electrode shows an increased presence of Mn on the anode surface with cycling. Mn dissolution is attributed to acid generated due to electrolyte oxidation during charge. The generated acid also attacks the SEI layer and leads to loss of active material at the anode. Hence, capacity fade of the spinel-based Li-ion cells can be attributed to (*i*) structural degradation at the cathode and (*ii*) loss of active materials at both electrodes due to electrolyte oxidation.

Acknowledgments

The authors are grateful for the financial support provided by National Reconnaissance Organization (NRO) under contract no. NRO-00-C-0134.

The University of South Carolina assisted in meeting the publication costs of this article.

References

1. P. Arora, R. E. White, and M. Doyle, *J. Electrochem. Soc.*, **145**, 3647 (1998).
2. M. C. Smart, B. V. Ratnakumar, S. Surampudi, Y. Wang, X. Zhang, and B. Fultz, *J. Electrochem. Soc.*, **146**, 3963 (1999).
3. D. Zhang, B. S. Haran, A. Durairajan, R. E. White, Y. Podrazhansky, and B. N. Popov, *J. Power Sources*, **91**, 122 (2000).
4. *Handbook of Batteries*, 2nd ed., D. Linden, Editor, pp. 36.44-48, McGraw-Hill, New York (1995).
5. D. Aurbach, M. D. Levi, K. Gamulski, B. Markovsky, G. Salitra, E. Levi, U. Heider, L. Heider, and R. Oesten, *J. Power Sources*, **81-82**, 472 (1999).
6. R. J. Gummow, A. de Kock, and M. M. Thackeray, *Solid State Ionics*, **69**, 59 (1994).
7. H. Huang, C. A. Vincent, and P. G. Bruce, *J. Electrochem. Soc.*, **146**, 3649 (1999).
8. Y. Xia, Y. Zhou, and M. Yoshio, *J. Electrochem. Soc.*, **144**, 2593 (1997).
9. E. Wang, D. Ofer, W. Bowden, N. Iltchev, T. Moses, and K. Brandt, *J. Electrochem. Soc.*, **147**, 4023 (2000).
10. Q. Wu, W. Lu, and J. Prakash, *J. Power Sources*, **88**, 237 (2000).
11. J. Cho and M. M. Thackeray, *J. Electrochem. Soc.*, **146**, 3577 (1999).
12. J. C. Hunter, *J. Solid State Chem.*, **39**, 142 (1981).